Phys. Lett. B 854 (2024) 138754

Contents lists available at ScienceDirect

Physics Letters B

journal homepage: www.elsevier.com/locate/physletb

Letter

The quark-mass dependence of the potential energy between static colour sources in the QCD vacuum with light and strange quarks

John Bulava [a], Francesco Knechtli [b,*], Vanessa Koch [b], Colin Morningstar [c], Michael Peardon [d]

[a] Fakultät für Physik und Astronomie, Institut für Theoretische Physik II, Ruhr-Universität Bochum, 44780 Bochum, Germany
[b] Department of Physics, University of Wuppertal, Gaußstrasse 20, 42119, Germany
[c] Department of Physics, Carnegie Mellon University, Pittsburgh, PA 15213, USA
[d] School of Mathematics, Trinity College Dublin, Ireland

ARTICLE INFO

Editor: B. Grinstein

ABSTRACT

The low-lying energy spectrum of the static-colour-source-anti-source system in a vacuum containing light and strange quarks is computed using lattice QCD for a range of different light quark masses. The resulting levels are described using a simple model Hamiltonian and the parameters in this model are extrapolated to the physical light-quark masses. In this framework, the QCD string tension is found to be $\sqrt{\sigma} = 445(3)_{\text{stat}}(6)_{\text{sys}}$ MeV.

1. Introduction

The energy levels of a static quark anti-quark pair $V_n(r)$ as a function of the interquark distance r probe Quantum Chromodynamics (QCD) at all scales. For very small distances $r \lesssim 0.1$ fm the potential can be computed by perturbation theory. At large distances the behaviour of the potential depends on the matter content. In pure-gauge theory at large separations, the potential can be modelled by an effective bosonic string. With dynamical quarks, the ground-state potential $V_0(r)$ flattens at large r due to the formation of a pair of static-light mesons ("light" refers here to the dynamical quarks). It was noted already in [1] that "the ground state potential therefore be called a static quark potential or a static meson potential". A first estimate of the distance where saturation of the ground state potential sets in was provided in [2]. Later, a model for string breaking as a mixing phenomenon between a string and a two-meson state was formulated in Ref. [3], which predicted for lighter quark mass the energy gap becomes larger and the width of the mixing region also expands. First observations of string breaking were made in the three-dimensional [4] and four-dimensional [5,6] SU(2) gauge-Higgs model with scalar matter fields. Evidence for string breaking in QCD with $N_f = 2$ quark flavours was shown in [7] for a sea quark mass slightly below the strange quark mass corresponding to $m_\pi \approx 650$ MeV. String breaking occurred for static-source separations of $r_c \approx 1.25$ fm. Our previous work [8] presented a computation of the three lowest potential energy levels in QCD with $N_f = 2 + 1$ quark flavours at quark masses corresponding to $m_\pi \approx 280$ MeV and $m_K \approx 460$ MeV. The computation was performed on the N200 gauge ensemble generated by the CLS consortium [9]. We found two string breaking distances $r_c \approx 1.22$ fm and $r_{c_s} \approx 1.29$ fm corresponding to the saturation of the potential levels by two static-light and two static-strange meson levels, respectively.

This work extends the analysis of Ref. [8] to study the quark-mass dependence by including two additional gauge ensembles with the same lattice spacing $a \approx 0.063$ fm and with one ensemble at a lighter quark mass and one heavier ensemble, covering a range of pion masses $m_\pi \in [200, 340]$ MeV. Ref. [8] showed the energy levels are modelled reliably by a simple three-state Hamiltonian with six parameters. One model parameter can be interpreted as a string tension. In this work we determine the quark-mass dependence of these model parameters. We introduce one more parameter in the model to include a curvature term proportional to $1/r$ as seen in the Cornell potential [10]. We extrapolate values of the seven parameters to the physical point following a trajectory where the sum of the bare quark masses is kept constant and close to its physical value.

The string tension enters as a parameter into models describing the fragmentation of partons into hadrons [11–14]. The so called "Lund model" [15] is implemented to describe hadronisation in the "Pythia" Monte-Carlo event generator [16]. In such models the string tension corresponds to a constant energy per unit length of the flux tube containing the colour field of a quark and anti-quark pair. The result of the present work provides input from first principles which could be used to refine these models by adding information on the excited states, for example.

* Corresponding author.
E-mail address: knechtli@physik.uni-wuppertal.de (F. Knechtli).

https://doi.org/10.1016/j.physletb.2024.138754
Received 6 March 2024; Received in revised form 20 May 2024; Accepted 23 May 2024
Available online 29 May 2024

Table 1
CLS ensembles [9,17] used in this work. N_{conf} is the number of configurations on which fermionic observables were measured. N^{W}_{conf} is the number of Wilson loop measurements, binned into N_{conf} bins. The third column gives the flow scale t_0 [18] in lattice units. The lattice sizes are $T = N_{\mathrm{t}}a$ in time and $L = N_{\mathrm{s}}a$ in space. The last three columns list the pion mass, the kaon mass and the value of $m_\pi L$ from [19].

label	N_{conf}	N^{W}_{conf}	t_0/a^2	N_{s}	N_{t}	m_π [MeV]	m_K [MeV]	$m_\pi L$
N203	94	752	5.1433(74)	48	128	340	440	5.4
N200	104	1664	5.1590(76)	48	128	280	460	4.4
D200	209	1117	5.1802(78)	64	128	200	480	4.2

The paper is organised as follows. The methodology of the lattice calculation, closely following the techniques used in our earlier work, is reviewed in Sec. 2. Section 3 introduces the simple model describing the dependence of the lowest energy levels on the static-colour-source separation, including the addition of the $1/r$ term. Having extracted the model parameters from the data at three values of the light quark mass, Section 4 establishes their dependence on the light quark dynamics and extrapolates to the physical quark-mass value. This is used to present the energy levels in the physical theory as the final result of the paper in Fig. 9. Our conclusions are presented in Section 5.

2. Methodology

To investigate the dependence of the static energies on quark mass, we extend our previous analysis to include three ensembles of gauge configurations generated by the CLS consortium [9,17]. These ensembles include the dynamics of $N_{\mathrm{f}} = 2+1$ flavours of non-perturbatively O(a) improved Wilson fermions [20] with a tree-level O(a^2) improved Lüscher–Weisz gauge action [21] and are described in Table 1. In addition to ensemble N200 analysed in Ref. [8], we consider one ensemble at a smaller value of the pion mass, D200 and one at a larger pion mass, N203. These ensembles have the same lattice spacing $a = 0.0633(4)(6)\,\mathrm{fm}$ (corresponding to an inverse bare gauge coupling $6/g_0^2 = \beta = 3.55$) [22]. The quark masses $m_{\mathrm{up}} = m_{\mathrm{down}} = m_l$ and $m_{\mathrm{strange}} = m_s$ vary along a chiral trajectory with constant sum of the bare quark masses. The bare quark masses were chosen such that the chiral trajectory approximately passes through the physical point [19]. Since the bare parameters corresponding to the physical point are only determined after completing the analysis of the trajectory, some discrepancy can remain. For the ensembles considered in this work, these quark mass mistunings have been computed in [19,22]. We are confident the effects these mistunings have on our analysis are small and subsequently neglect them. We introduce the quark-mass parameter,

$$\mu_l = \frac{3m_\pi^2}{m_\pi^2 + 2m_K^2}\,, \tag{1}$$

where m_π, m_K are the pion and kaon masses. We take these meson masses in lattice units from Ref. [19] to compute μ_l. To leading-order in chiral perturbation theory $\mu_l \approx \frac{3m_l}{2m_l+m_s}$ and so along a trajectory which holds the sum of the quark masses $2m_l + m_s$ fixed, μ_l is proportional to the light quark mass m_l. At the $N_{\mathrm{f}} = 3$ flavour-symmetric point $\mu_l = 1$ holds. For physical quark masses and correcting for isospin-breaking effects, $m_\pi = 134.8\,\mathrm{MeV}$, $m_K = 494.2\,\mathrm{MeV}$ [19] and consequently $\mu_l^{\mathrm{phys}} = 0.1076$. To mitigate against topological freezing, open boundary conditions in time [23] are used. Reweighting factors [24] are included in the analysis of observables to modify the action to the appropriate one. Statistical uncertainties are determined by the Γ-method [25,26]. There are no measurable autocorrelations in our data and we do not add a tail to the autocorrelation function.

We compute the allowed energies of a system comprising a static quark at spatial position $\vec{x}$ and a static anti-quark at position $\vec{y}$ as a function of separation $\vec{r} = \vec{y} - \vec{x}$. The calculation involves the computation of a matrix of time-correlation functions $C(\vec{r}, t)$ between states created by a flux tube operator or states consisting of a static meson and anti-meson pair with isopin zero. In a theory with degenerate dynamical up and down light quarks and a strange-quark, two sets of mesons are formed by combining a static source with either a light or strange quark, giving the static-light or static-strange mesons. $C(\vec{r}, t)$, the relevant matrix correlation function needed to study this spectrum is shown schematically in Fig. 1. Explicit expressions for the interpolation operators of string and two-meson states are given in [8].

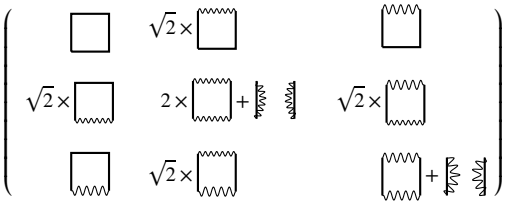

Fig. 1. Schematic representation of the string breaking mixing matrix.

All gauge links in the interpolating operators are smeared using HYP2 parameters [27–31] $\alpha_1 = 1.0, \alpha_2 = 1.0, \alpha_3 = 0.5$. For the string operators, 15 and 20 levels of spatial HYP smearing with parameters $\alpha_2 = 0.6$, $\alpha_3 = 0.3$ [31] are used. To increase spatial resolution of the energies in the string breaking regions we use on- and off-axis distances $\vec{r}$. For off-axis displacements, gauge-link paths which follow the straight line connecting the static source and anti-source as closely as possible are constructed [32], using the Bresenham algorithm [33]. Following this closest path significantly enhances the overlap between creation operator and physical string states.

Two distinct computational techniques to compute quark propagators (represented by the wiggly lines in Fig. 1) are needed. We refer to propagators starting and terminating on the same time slice $t_s = t_f$ as "relative", while quark propagators with $t_s \neq t_f$ are called "fixed". Evaluation of quark line diagrams uses the stochastic LapH method [34], based on the distillation quark-smearing technique [35]. Distillation projects the quark fields on a time-slice into the space spanned by the lowest N_v eigenmodes of the three-dimensional gauge-covariant Laplace operator, constructed from stout-smeared gauge-links [36] with parameters $\rho = 0.1$, $n_\rho = 36$. Propagators between distillation spaces are estimated using stochastic LapH, with the variance reduced by dilution [37–39]. Fixed quark propagators are evaluated on two source times $t_s/a = \{32, 52\}$ using full time and spin dilution with interlace-8 LapH eigenvector dilution, denoted collectively by (TF, SF, LI8) [34]. Relative quark propagators are evaluated on all source times $t_s/a \in \{32, 33, \ldots, 95\}$ using interlace-8 time and full spin dilution with interlace-8 LapH eigenvector dilution, labelled (TI8,SF,LI8). A total of $S \cdot L \cdot N_r \cdot t_s + S \cdot T \cdot L \cdot N_r$ (fixed+relative) solutions of the Dirac equation (inversions) are required per gauge configuration for each quark flavour. Here N_r denotes the number of random vectors in the space defined by the dilution projectors. For our choice of dilution schemes the number of inversions per quark flavour is $4 \cdot 8 \cdot N_r \cdot 2 + 4 \cdot 8 \cdot 8 \cdot N_r$ (fixed+relative). These parameters are summarised in Table 2. Note correlation functions for off-axis static source separations are easy to compute using relative and fixed quark propagators, unlike the off-axis gauge-link paths.

Table 2
The number of Laplacian eigenmodes N_v spanning the distillation space and the inversion costs for all ensembles used in this calculation. For each type of quark line and flavour, the number of stochastic vectors in the space defined by the dilution projectors and the corresponding total number of inversions is given. The source times and the dilution schemes employed are specified in the text.

			light		strange	
	N_v	Type	N_r	n_{inv}	N_r	n_{inv}
N203	192	fixed	5	320	2	128
		relative	2	512	1	256
N200	192	fixed	5	320	2	128
		relative	2	512	1	256
D200	448	fixed	7	448	2	128
		relative	3	768	1	256

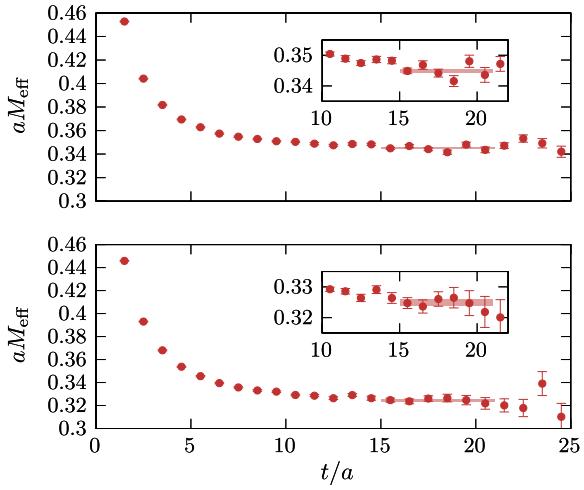

Fig. 2. Effective masses of the static-light (bottom) and static-strange (top) mesons on the ensemble D200. The horizontal bands indicate the time intervals used and energies obtained from a single exponential fit to the corresponding correlators.

We start by extracting energies of the static-light meson $E_{\bar{Q}l}$ and static-strange mesons $E_{\bar{Q}s}$. The thresholds for the avoided level crossings of string breaking are given by twice these energies. When an energy level reaches one of these thresholds, the state formed by a meson anti-meson pair becomes energetically more favourable. The static-light and static-strange energies are obtained from single exponential correlated fits to the time-correlation function $C_{\bar{Q}l}(t)$ and $C_{\bar{Q}s}(t)$ of a static-light meson and a static-strange meson respectively. For all ensembles fits are carried out in the time interval $[15, 21]$ in lattice units. Fig. 2 shows the effective masses $aM_{\text{eff}}(t + a/2) = \ln[C(t)/C(t + a)]$ (points) as a function of t/a for ensemble D200. The top and bottom panels show the static-strange and static-light mesons respectively. Horizontal bands indicate the values of $aE_{\bar{Q}l}$ and $aE_{\bar{Q}s}$ extracted from the correlator fits extending over the fitted time range.

For each fixed inter-quark separation $r = |\vec{r}|$ we solve a generalized eigenvalue problem (GEVP) using the correlation matrix of Fig. 1

$$C(t)\, v_n(t, t_0) = \lambda_n(t, t_0)\, C(t_0)\, v_n(t, t_0)\,, \tag{2}$$

to extract the potential energies for $n = 0, 1, 2$ and $t > t_0$. We fix $t_0 = 5a$ for all ensembles. To ensure numerical stability of the analysis we first prune [40–42] the correlation matrix from size 4×4 down to 3×3, replacing $C(t)$ with

$$C^{(3)}(t) = \bar{U}^\dagger \bar{C}(t_0)^{-1/2} C(t) \bar{C}(t_0)^{-1/2} \bar{U}\,. \tag{3}$$

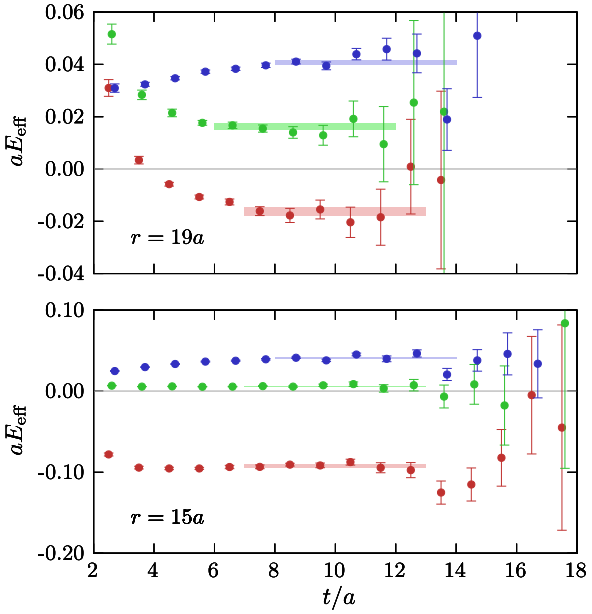

Fig. 3. Examples of effective masses of the ratios Eq. (5) on the ensemble D200 at two distances as indicated in the plots. The horizontal bands correspond to the energies $V_n(r) - 2E_{\bar{Q}l}$, $n = 0, 1, 2$ extracted from exponential fits to the ratios and extend over the fitted time interval.

$\bar{U}$ contains the three most significant eigenvectors at $t_0 + a$. The bar in $\bar{U}$ and $\bar{C}(t_0)$ indicates these matrices are determined on the average over gauge configurations. Then we solve the GEVP in Eq. (2) at time $t = t_d = 10a$, which is fixed for all the ensembles. Using the three eigenvectors $v_i(t_0, t_d)$, $i = 0, 1, 2$ we project to a single correlation function ("fixed GEVP") by computing

$$\hat{C}_{ij}(t) = \left(v_i(t_0, t_d), C^{(3)}(t) v_j(t_0, t_d)\right), \tag{4}$$

where the parentheses denote the inner product over the components of the eigenvectors. The statistical precision of our analysis is improved by exploiting the beneficial covariance between $\hat{C}$ and the static-light meson correlator $C_{\bar{Q}l}(t)$. The correlation function ratios

$$R_n(t) = \frac{\hat{C}_{nn}(t)}{C^2_{\bar{Q}l}(t)}\,, \tag{5}$$

for $n = 0, 1, 2$ are then computed and fits to a single exponential with time dependence $\exp(-t(V_n - 2E_{\bar{Q}l}))$ are performed. In these ratios, energy levels become renormalised by the subtraction of twice the divergent static-light energy since the additive self-energy contribution of the static-quarks exactly cancels. The fit ranges $[t_{\min}/a, t_{\max}/a]$ are carefully chosen in each case by inspection. Any remaining systematic uncertainty mainly comes from $t_{\min}/a$ dependence and we choose values of $t_{\min}/a$ such that these effects are within the limits of statistical precision. Finally we set $t_{\max} = t_{\min} + 6a$. Fig. 3 shows examples of effective masses $aE_{\text{eff}}(t + a/2) = \ln[R_n(t)/R_n(t + a)]$ for $n = 0, 1, 2$ for two on-axis inter-quark separations $r = 15a$ and $r = 19a$ on the ensemble D200. Note the effective masses derived from ratios in Eq. (5) can approach their plateau values from below. The bands indicate the energy values from the exponential fits of R_n and extend over the fitted time ranges. The distance $15a$ (bottom plot in Fig. 3) is the smallest distance down to which we can reliably determine the excited states. The separation $19a$ (top plot in Fig. 3) is in the middle of the first string-breaking region where the ground state and first excited state potential levels would cross. Notice all three energy levels are very close at $r = 19a$, and yet the GEVP is able to disentangle the three levels very efficiently.

Fig. 4 shows the three lowest potential energy levels $a(V_n - 2E_{\bar{Q}l})$ in lattice units as a function of the distance r/a in the region where

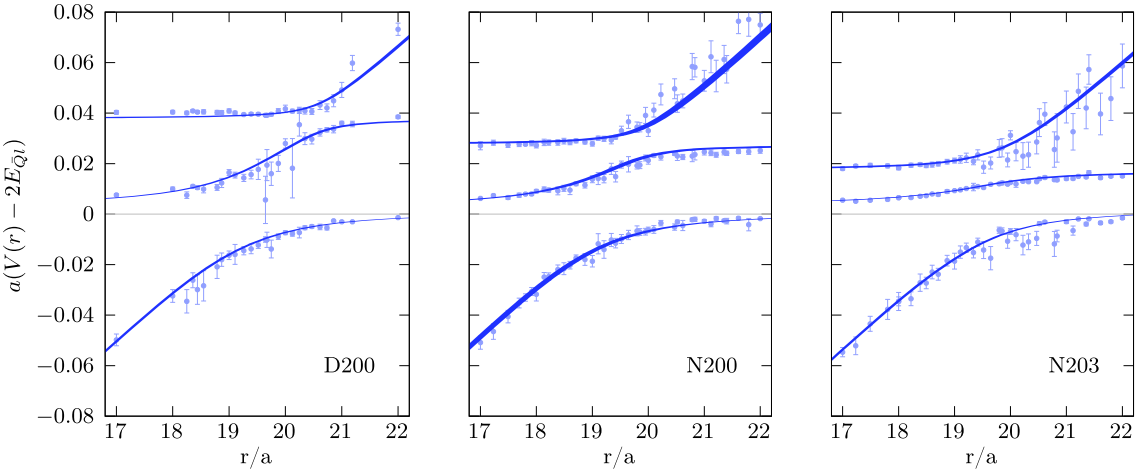

Fig. 4. The energy levels extracted from the GEVP analysis for separations in the range $r/a \in [17, 22]$ for the three ensembles described in Table 1. The data include off-axis separations. The bands indicate the energies extracted from a fit of data to the seven-parameter model of Eq. (6).

Table 3
Distance ranges $[r_1(n)/a, r_2(n)/a]$ used for the 7-parameter model fits to ground ($n = 0$), first ($n = 1$) and second excited state ($n = 2$).

id	$n = 0$	$n = 1$	$n = 2$
N203	[4, 24]	[11, 24]	[11, 24]
N200	[4, 24]	[11, 24]	[11, 24]
D200	[4, 27]	[15, 27]	[15, 27]

string breaking occurs for each of the three ensembles described in Table 1. Along our trajectory of decreasing light quark mass and increasing strange quark mass the energy gap between the first and second string breaking increases. In order to have a better resolution of the avoided level crossings we include off-axis distances. Some fluctuations in the size of the statistical errors can be seen especially for the off-axis distances. For on-axis distances we profit from self-averaging due to the cubic symmetry.

3. Model

The model used in Ref. [8] is extended to fit the data at smaller separations by the inclusion of a Cornell $1/r$ term. The three-state model Hamiltonian becomes

$$H(r) = \begin{pmatrix} \hat{V}(r) & \sqrt{2}g_l & g_s \\ \sqrt{2}g_l & \hat{E}_1 & 0 \\ g_s & 0 & \hat{E}_2 \end{pmatrix}, \hat{V}(r) = \hat{V}_0 + \sigma r + \gamma/r\,. \tag{6}$$

After introducing a parameter γ for the $1/r$ term, the new model has seven parameters, labelled $\{\hat{E}_1, \hat{E}_2, g_l, g_s, \sigma, \hat{V}_0, \gamma\}$. The diagonal entries in Eq. (6), $\hat{V}(r)$, $\hat{E}_1$, $\hat{E}_2$ are the asymptotic energy levels for $r \to \infty$ up to $O(r^{-1})$. When there are N_l degenerate light flavours in the mixing matrix elements between string and two-meson states of the model Hamiltonian, a flavour factor $\sqrt{N_l}$ multiplies the mixing coefficient g_l, in analogy to the corresponding flavour factor in Fig. 1. For $N_l = 2$ the factor $\sqrt{2}$ in the three-state model Hamiltonian Eq. (6) can be derived from a four-state Hamiltonian with non-degenerate up and down quarks by taking the limit of degenerate light quarks.

The dependence of the three eigenvalues $e_n(r), n = 0, 1, 2$ of the model Hamiltonian Eq. (6) on the distance r is fitted to the three lowest potential energy levels $V_n(r)$ determined from the data. These levels are normalised by subtracting twice the energy of the static-light meson $2E_{\bar{Q}l}$. Hence the fitted eigenvalues inherit this normalisation, which removes the divergent self-energy contribution from the temporal static-quark lines. The model fit parameters in Eq. (6) are obtained by minimisation of the correlated χ^2,

$$\chi^2_{\text{corr}} = \sum_{n,m=0}^{2} \sum_{r=r_1(n)}^{r_2(n)} \sum_{r'=r_1(m)}^{r_2(m)} \Big(V_n(r) - 2E_{\bar{Q}l} - e_n(r)\Big) \bar{C}^{-1} \Big(V_m(r') - 2E_{\bar{Q}l} - e_m(r')\Big), \tag{7}$$

where $\bar{C}^{-1}$ is the inverse of the covariance matrix for the potential levels V_n. The matrix $\bar{C}$ is determined by the Γ-method. For each pair of potential levels we compute the squared statistical errors of their sum and their difference. The covariance between two levels is obtained from the difference of these two squared errors. In order to obtain a positive matrix we switch off the autocorrelations between the potential levels when computing $\bar{C}$. The distance ranges $[r_1(n), r_2(n)]$ used to fit potential levels V_n on individual ensembles are given in Table 3. The minimal distance for the ground state V_0 is set to $4a$ in order to be sensitive to the Cornell $1/r$-term. For the first and second excited states, V_1 and V_2 respectively, the minimal distance is chosen so the energy gap to the ground state is smaller than $2m_\pi$. By this choice we avoid fitting our excited state levels at too small distances where there could be unresolved intermediate energy levels in our analysis. For ensembles N200 and N203 we set the maximal distance for the fit equal to $L/2$. Potential values at distances larger than $L/2$ suffer from finite volume effects and are not considered. We impose a cut on the covariance matrix C of the potential levels using a singular value decomposition. Eigenvalues of C less than 10^{-4} times the maximal eigenvalue are removed from the inverse covariance which we denote by $\bar{C}^{-1}$ in Eq. (7). We investigated the dependence of the fit parameters on this cut parameter and found this a reasonable choice; cuts of 10^{-5} or 10^{-3} times the maximal eigenvalues give consistent results.

In Fig. 4 the bands show the seven-parameter model fits to Eq. (6) for each of the three ensembles analyzed in this work and including statistical errors. We see that the model describes our data very well in the region where string breaking happens.

4. Mass dependence and physical point

With three ensembles generated with different light and strange quark masses, the mass dependence of the model and its parameters can be investigated and an extrapolation to the physical values of the quark masses attempted. To begin, the difference between the static-light and static-strange meson masses was determined and a linear extrapolation to the physical light quark mass performed. The result of this extrapolation can be seen in Fig. 5. The subtraction removes the divergent static source energy, yielding a splitting with a well-defined continuum limit. We performed a fit to a simple model assuming linear dependence of

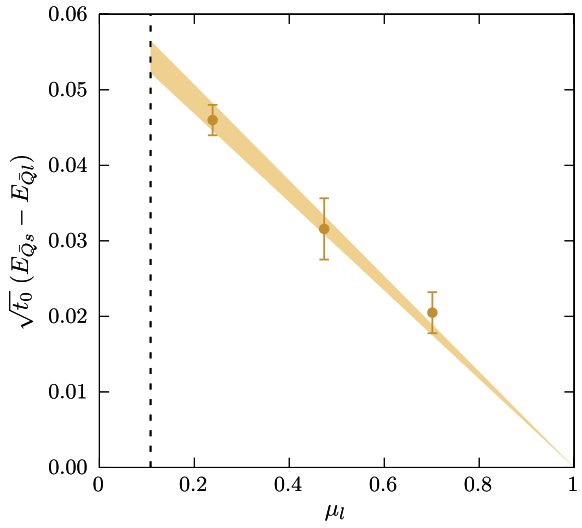

Fig. 5. Dependence of the mass difference between the static-light and static-strange meson masses on the light-quark mass parameter μ_l of Eq. (1).

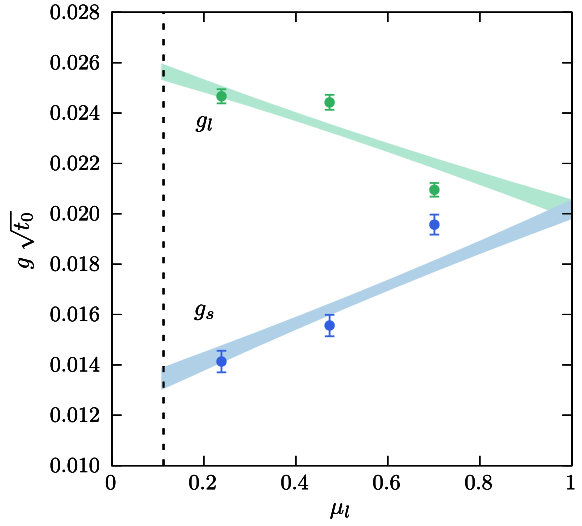

Fig. 6. Dependence of the mixing parameters, g_l and g_s on the light-quark mass parameter, μ_l of Eq. (1). The vertical line indicates the physical light-quark mass ratio.

this splitting on the light-quark mass parameter, μ_l away from the three-flavour symmetric point corresponding to $\mu_l = 1$. The data clearly shows agreement with this simple behaviour. Extrapolation to $\mu_l^{\rm phys}$ yields $\sqrt{t_0}(E_{\bar{Q}s} - E_{\bar{Q}l}) = 0.054(2)$ which gives $E_{\bar{Q}s} - E_{\bar{Q}l} = 74(3)_{\rm stat}(1)_{\rm sys}$ MeV using $\sqrt{t_0} = 0.1443(7)(13)$ fm [22]. This compares with the experimentally determined value of the mass difference, averaged over isospin for the B_s and B mesons of 87.42(14) MeV [43]. The discrepancy is most likely due to finite heavy-quark-mass effects, neglected in this calculation. Other possible effects include finite-lattice-spacing artefacts and systematic uncertainty in the light- and strange-quark mass determinations.

The two mixing parameters, g_l and g_s of Eq. (6) determined at the three light-quark values are displayed in Fig. 6. Without a robust prediction from theory, their light-quark mass dependence was again modelled assuming a simple linear behaviour, cf. [44] with the two straight-lines constrained to a common value at the flavour-symmetric point, corresponding to $\mu_l = 1$. For this fit, $\chi^2/n_{\rm df} = 16.8$ and some tension between the data and the model is seen close to the three-degenerate-flavour point. In the absence of a more detailed model for this mass dependence, the phenomenon was not investigated further. As seen clearly in this figure however, the two mixing parameters, g_l and g_s differ by a factor of almost two for physical values of the quark masses. Assuming linear behaviour yields extrapolated values of $g_{l,s}$ at the physical light-quark mass ratio of

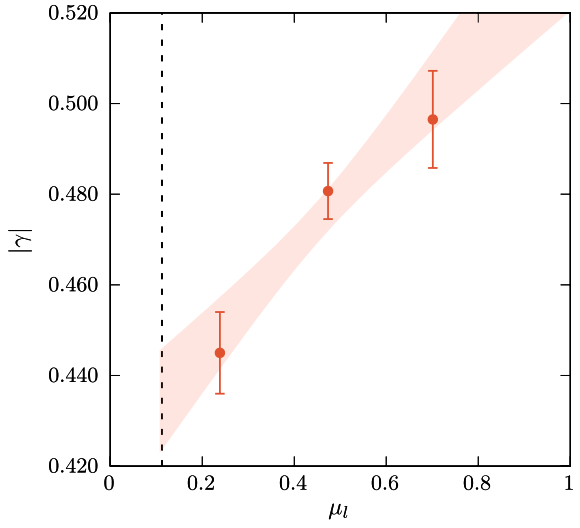

Fig. 7. Light-quark mass-dependence of the coefficient of the dimensionless $1/r$ Cornell potential term from fits to the model of Eq. (6). The vertical line indicates the physical light-quark mass ratio.

$$g_l\sqrt{t_0} = 0.0256(3), \qquad g_l = 35.0\,(5)_{\rm stat}(3)_{\rm sys}\,\text{MeV}$$
$$g_s\sqrt{t_0} = 0.0134(4), \qquad g_s = 18.3\,(6)_{\rm stat}(2)_{\rm sys}\,\text{MeV}. \tag{8}$$

Fig. 7 shows the light-quark mass dependence of the coefficient γ weighting the $1/r$ term in $\hat{V}(r)$ modelling the gluonic flux-tube in Eq. (6). $|\gamma|$ is plotted for clarity. Significant mass dependence in this term is observed and the value extrapolated to the physical point is found to be

$$\gamma^{\rm phys} = -0.434(11). \tag{9}$$

The uncertainty is purely statistical as there is no scale dependence on this dimensionless parameter. Understanding the mass dependence in detail would require closer study of the transition from the short-distance behaviour of the static potential into the string-breaking region and is beyond the scope of this first study.

The dependence of the string tension on μ_l is seen in Fig. 8, along with two simple models to describe this behaviour and extrapolate to the physical point. The simplest model asserts no dependence of σ on μ_l while the second model assumes linear dependence. The change in σ over the full range of μ_l is seen to be mild and is only a few percent from the three-flavour symmetric theory to the physical point. The mass dependence is not described very well by either model and the statistical uncertainties at the physical point from the two fits do not capture the discrepancy between the models. Using the linear model to give a central value at the physical point but assigning a systematic uncertainty from the difference between the extrapolated values in the two models yields

$$\sigma t_0 = 0.1061(7)(20), \quad \sqrt{\sigma} = 445(3)_{\rm stat}(6)_{\rm sys}\,\text{MeV}, \tag{10}$$

where the uncertainty quoted includes both statistical and extrapolation uncertainties from our determination of σt_0 combined in quadrature with the scale-setting uncertainty from $\sqrt{t_0} = 0.1443(7)(13)$ fm [22]. Table 4 shows the correlations between the model parameters after extrapolating to the physical quark masses. Some parameters are seen to be strongly correlated, in particular the three coefficients in $\hat{V}(r)$ have high statistical correlations, including a pair with a correlation of 92%.

Table 4
Summary of the model parameters of Eq. (6) after extrapolation to the physical quark masses. The left-hand table shows the normalised correlation coefficients between all parameters. Their values and statistical uncertainty are given in the right table.

	$\hat{E}_2$	g_l	g_s	σ	$\hat{V}_0$	γ
$\hat{E}_1$	0.12	0.23	-0.02	-0.01	-0.01	0.10
$\hat{E}_2$		0.05	-0.11	0.09	0.07	-0.07
g_l			0.29	0.04	-0.07	0.04
g_s				0.06	-0.13	0.13
σ					-0.92	0.70
$\hat{V}_0$						-0.85

Parameter	Best Fit
$\hat{E}_1\sqrt{t_0}$	0.0034(3)
$\hat{E}_2\sqrt{t_0}$	0.1005(7)
$g_l\sqrt{t_0}$	0.0256(3)
$g_s\sqrt{t_0}$	0.0134(4)
σt_0	0.1061(7)
$\hat{V}_0\sqrt{t_0}$	-0.835(7)
γ	-0.434(11)

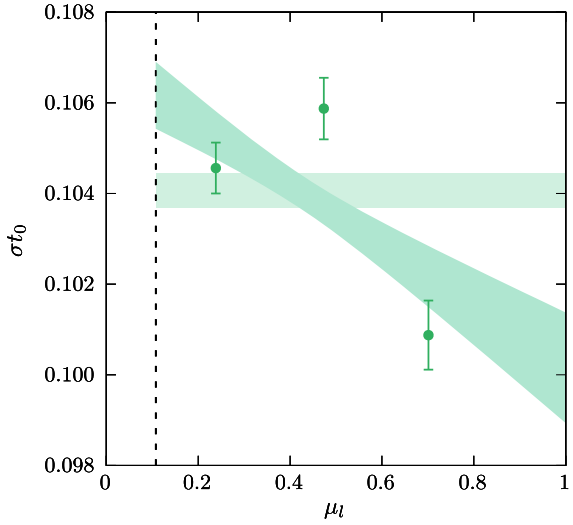

Fig. 8. Dependence of the string tension on the light and strange quark masses. μ_l, the dimensionless light quark mass parameter is defined in Eq. (1). The two bands indicate extrapolating fits using constant or linear dependence. The physical value of the mass ratio, μ_l^{phys} is indicated by the vertical dashed line.

The right table in Table 4 lists the model parameters with their statistical errors after linear extrapolations in μ_l (best fit) to the physical quark masses.

Using the model with parameters extrapolated to the physical point, the dependence of the energy spectrum of the static source-anti-source system on source separation in the presence of physical up, down and strange quarks can be computed and is presented in Fig. 9. The zero of the potential is fixed by subtracting twice the energy of the static-light system, which makes the ground-state energy at large separations vanish asymptotically. The excited states are not displayed at short separations, where the basis of operators may not couple efficiently to possible multi-meson states and so the determination of the spectrum in this range for this calculation is uncertain.

The string-breaking distances, $r_l^\star$ and $r_s^\star$ are indicated by two vertical bands in Fig. 9. These distances are derived from the model by determining the static source-sink separation where $\hat{V}(r)$ is equal to the asymptotic energy of two static-light (for $r_l^\star$) or static-strange (for $r_s^\star$) mesons. This yields

$$r_l^\star = 8.39(3)\sqrt{t_0} = 1.211(7)_{\text{stat}}(11)_{\text{sys}}\ \text{fm},$$
$$r_s^\star = 9.26(2)\sqrt{t_0} = 1.336(7)_{\text{stat}}(12)_{\text{sys}}\ \text{fm}. \quad (11)$$

Again, the values quoted in physical units include estimates of the uncertainties arising both from limits to the statistical precision of our calculation and systematic uncertainty from setting the physical scale.

5. Conclusions

This paper extends the analysis of Ref. [8] to investigate the light-quark mass dependence of the potential energy of a system of a static colour-anti-colour source pair. The three lowest energy levels in the resulting spectrum are determined up to the scale where mixing between states resembling a gluon string and two static-light or static-strange mesons is largest. A robust determination is achieved by computing correlations within a suitable variational basis of interpolating fields and solving the resulting generalised eigenvalue problem. A simple model of the spectrum is presented, starting from the Cornell potential and allowing mixing with the asymptotic static-meson states.

Using the new data from calculations with different light-quark masses, an extrapolation of the model parameters to the physical quark mass values is performed, enabling us to predict the physical potential in QCD with dynamical light and strange quarks and to give a simple parameterisation of this potential and its excitations. Perhaps the most studied parameter is the string tension where the value determined in this work is seen in Eq. (10). In comparison, the string tension in pure-gauge theory is in the range $\sigma t_0 \in [0.143, 0.159]$. These values are computed using data on the deconfining temperature T_c/σ compiled in [45] combined with $T_c r_0$ from [45] and $r_0/\sqrt{t_0}$ from [46]. These results are almost 40% higher than this work for $N_{\text{f}} = 2+1$ QCD. A recent determination in $N_{\text{f}} = 2+1+1$ QCD [47] gives $\sqrt{\sigma} = 467(7)$ MeV or 482(7) MeV depending on the type of Cornell fits to the ground state potential used for distances below 1 fm. This shows there are important physical effects in the string tension generated by the phenomenon of string breaking.

Our data for the three lowest energy levels of the static potential can be well fitted assuming the simple model in Eq. (6). Other phenomenological models [48] could motivate further investigations.

Declaration of competing interest

The authors declare that they have no known competing financial interests or personal relationships that could have appeared to influence the work reported in this paper.

Data availability

Data will be made available on request.

Acknowledgements

We thank Christoph Hanhart, Paul Pütz and Tommaso Scirpa for helpful discussions of the mass extrapolations and Tomasz Korzec for help with the data analysis. We are grateful to Tom DeGrand for feedback. We thank Ben Hörz and Graham Moir for their contributions at an early stage. The authors gratefully acknowledge the Gauss Centre for Supercomputing e.V. (www.gauss-centre.eu) for funding this project by providing computing time on the GCS Supercomputer JUQUEEN [49] at

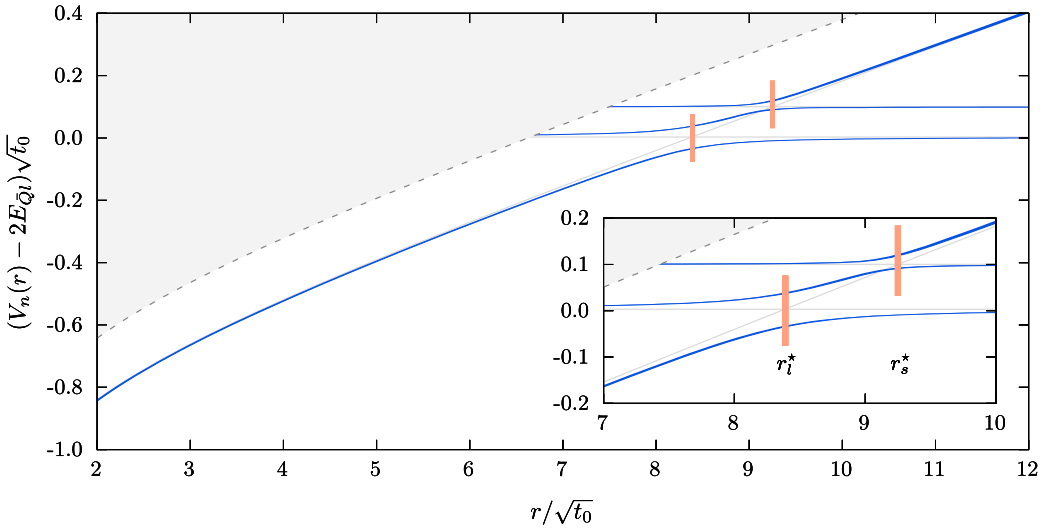

Fig. 9. The energy spectrum of the static source-anti-source system from the model of Eq. (6) with parameters extrapolated in light-quark mass to the physical point. The grey region denotes the energy regime where two-pion creation operators would be needed for a robust determination of higher-lying states. The breaking distances $r_l^\star$ and $r_s^\star$ computed in the model are indicated by the two vertical bands.

Jülich Supercomputing Centre (JSC). The code for the calculations using the stochastic LapH method is built on the USQCD QDP++/Chroma library [50]. The statistical error analysis has been performed with an internal package of the ALPHA Collaboration. The work is supported by the German Research Foundation (DFG) research unit FOR5269 "Future methods for studying confined gluons in QCD". C.M. acknowledges support from the U.S. National Science Foundation (NSF) through award PHY-2209167. This work was supported by the STRONG-2020 project, funded by the European Community Horizon 2020 research and innovation programme under grant agreement 824093.

References

[1] R. Sommer, Beauty physics in lattice gauge theory, Phys. Rep. 275 (1996) 1–47, https://doi.org/10.1016/0370-1573(96)00028-2, arXiv:hep-lat/9401037.
[2] C. Alexandrou, S. Gusken, F. Jegerlehner, K. Schilling, R. Sommer, The static approximation of heavy - light quark systems: a systematic lattice study, Nucl. Phys. B 414 (1994) 815–855, https://doi.org/10.1016/0550-3213(94)90262-3, arXiv:hep-lat/9211042.
[3] I.T. Drummond, Strong coupling model for string breaking on the lattice, Phys. Lett. B 434 (1998) 92–98, https://doi.org/10.1016/S0370-2693(98)00747-3, arXiv:hep-lat/9805012.
[4] O. Philipsen, H. Wittig, String breaking in nonAbelian gauge theories with fundamental matter fields, Phys. Rev. Lett. 81 (1998) 4056–4059, https://doi.org/10.1103/PhysRevLett.81.4056, Erratum: Phys. Rev. Lett. 83 (1999) 2684, arXiv:hep-lat/9807020.
[5] F. Knechtli, R. Sommer, String breaking in SU(2) gauge theory with scalar matter fields, Phys. Lett. B 440 (1998) 345–352, https://doi.org/10.1016/S0370-2693(98)01098-3, Erratum: Phys. Lett. B 454 (1999) 399, arXiv:hep-lat/9807022.
[6] F. Knechtli, R. Sommer, String breaking as a mixing phenomenon in the SU(2) Higgs model, Nucl. Phys. B 590 (2000) 309–328, https://doi.org/10.1016/S0550-3213(00)00470-3, arXiv:hep-lat/0005021.
[7] G.S. Bali, H. Neff, T. Duessel, T. Lippert, K. Schilling, Observation of string breaking in QCD, Phys. Rev. D 71 (2005) 114513, https://doi.org/10.1103/PhysRevD.71.114513, arXiv:hep-lat/0505012.
[8] J. Bulava, B. Hörz, F. Knechtli, V. Koch, G. Moir, C. Morningstar, M. Peardon, String breaking by light and strange quarks in QCD, Phys. Lett. B 793 (2019) 493–498, https://doi.org/10.1016/j.physletb.2019.05.018, arXiv:1902.04006.
[9] M. Bruno, et al., Simulation of QCD with $N_f = 2 + 1$ flavors of non-perturbatively improved Wilson fermions, J. High Energy Phys. 02 (2015) 043, https://doi.org/10.1007/JHEP02(2015)043, arXiv:1411.3982.
[10] E. Eichten, K. Gottfried, T. Kinoshita, K.D. Lane, T.-M. Yan, Charmonium: comparison with experiment, Phys. Rev. D 21 (1980) 203, https://doi.org/10.1103/PhysRevD.21.203.
[11] B. Andersson, G. Gustafson, G. Ingelman, T. Sjostrand, Parton fragmentation and string dynamics, Phys. Rep. 97 (1983) 31–145, https://doi.org/10.1016/0370-1573(83)90080-7.
[12] B. Andersson, G. Gustafson, C. Peterson, A semiclassical model for quark jet fragmentation, Z. Phys. C 1 (1979) 105, https://doi.org/10.1007/BF01450386.
[13] B. Andersson, G. Gustafson, B. Soderberg, A general model for jet fragmentation, Z. Phys. C 20 (1983) 317, https://doi.org/10.1007/BF01407824.
[14] T. Sjostrand, Jet fragmentation of nearby partons, Nucl. Phys. B 248 (1984) 469–502, https://doi.org/10.1016/0550-3213(84)90607-2.
[15] B. Andersson, The Lund Model, Cambridge Monographs on Particle Physics, Nuclear Physics and Cosmology, Cambridge University Press, 2023.
[16] T. Sjostrand, S. Mrenna, P.Z. Skands, PYTHIA 6.4 physics and manual, J. High Energy Phys. 05 (2006) 026, https://doi.org/10.1088/1126-6708/2006/05/026, arXiv:hep-ph/0603175.
[17] G.S. Bali, E.E. Scholz, J. Simeth, W. Söldner, Lattice simulations with $N_f = 2 + 1$ improved Wilson fermions at a fixed strange quark mass, Phys. Rev. D 94 (7) (2016) 074501, https://doi.org/10.1103/PhysRevD.94.074501, arXiv:1606.09039.
[18] M. Lüscher, Properties and uses of the Wilson flow in lattice QCD, J. High Energy Phys. 08 (2010) 071, https://doi.org/10.1007/JHEP08(2010)071, Erratum: J. High Energy Phys. 03 (2014) 092, arXiv:1006.4518.
[19] M. Bruno, T. Korzec, S. Schaefer, Setting the scale for the CLS 2 + 1 flavor ensembles, Phys. Rev. D 95 (7) (2017) 074504, https://doi.org/10.1103/PhysRevD.95.074504, arXiv:1608.08900.
[20] J. Bulava, S. Schaefer, Improvement of $N_f = 3$ lattice QCD with Wilson fermions and tree-level improved gauge action, Nucl. Phys. B 874 (2013) 188–197, https://doi.org/10.1016/j.nuclphysb.2013.05.019, arXiv:1304.7093.
[21] M. Lüscher, P. Weisz, On-shell improved lattice gauge theories, Commun. Math. Phys. 97 (1985) 59, https://doi.org/10.1007/BF01206178, Erratum: Commun. Math. Phys. 98 (1985) 433.
[22] B. Strassberger, et al., Scale setting for CLS 2+1 simulations, PoS LATTICE2021 (2022) 135, https://doi.org/10.22323/1.396.0135, arXiv:2112.06696.
[23] Martin Lüscher, Stefan Schaefer, Lattice QCD without topology barriers, J. High Energy Phys. 07 (2011) 036, https://doi.org/10.1007/JHEP07(2011)036, arXiv:1105.4749.
[24] M. Lüscher, S. Schaefer, Lattice QCD with open boundary conditions and twisted-mass reweighting, Comput. Phys. Commun. 184 (2013) 519–528, https://doi.org/10.1016/j.cpc.2012.10.003, arXiv:1206.2809.
[25] U. Wolff, Monte Carlo errors with less errors, Comput. Phys. Commun. 156 (2004) 143–153, https://doi.org/10.1016/S0010-4655(03)00467-3, Erratum: Comput. Phys. Commun. 176 (2007) 383, arXiv:hep-lat/0306017.
[26] S. Schaefer, R. Sommer, F. Virotta, Critical slowing down and error analysis in lattice QCD simulations, Nucl. Phys. B 845 (2011) 93–119, https://doi.org/10.1016/j.nuclphysb.2010.11.020, arXiv:1009.5228.
[27] A. Hasenfratz, F. Knechtli, Flavor symmetry and the static potential with hypercubic blocking, Phys. Rev. D 64 (2001) 034504, https://doi.org/10.1103/PhysRevD.64.034504, arXiv:hep-lat/0103029.
[28] M. Della Morte, S. Dürr, J. Heitger, H. Molke, J. Rolf, A. Shindler, R. Sommer, Static quarks with improved statistical precision, Nucl. Phys. B, Proc. Suppl. 129 (2004) 346–348, https://doi.org/10.1016/S0920-5632(03)02577-5, arXiv:hep-lat/0309080.
[29] M. Della Morte, A. Shindler, R. Sommer, On lattice actions for static quarks, J. High Energy Phys. 08 (2005) 051, https://doi.org/10.1088/1126-6708/2005/08/051, arXiv:hep-lat/0506008.
[30] A. Grimbach, D. Guazzini, F. Knechtli, F. Palombi, O(a) improvement of the HYP static axial and vector currents at one-loop order of perturbation theory, J. High Energy Phys. 03 (2008) 039, https://doi.org/10.1088/1126-6708/2008/03/039, arXiv:0802.0862.

[31] M. Donnellan, F. Knechtli, B. Leder, R. Sommer, Determination of the static potential with dynamical fermions, Nucl. Phys. B 849 (2011) 45–63, https://doi.org/10.1016/j.nuclphysb.2011.03.013, arXiv:1012.3037.

[32] B. Bolder, T. Struckmann, G.S. Bali, N. Eicker, T. Lippert, B. Orth, K. Schilling, P. Ueberholz, A high precision study of the Q anti-Q potential from Wilson loops in the regime of string breaking, Phys. Rev. D 63 (2001) 074504, https://doi.org/10.1103/PhysRevD.63.074504, arXiv:hep-lat/0005018.

[33] J.E. Bresenham, Algorithm for computer control of a digital plotter, IBM Syst. J. 4 (1965) 25–30.

[34] C. Morningstar, J. Bulava, J. Foley, K.J. Juge, D. Lenkner, M. Peardon, C.H. Wong, Improved stochastic estimation of quark propagation with Laplacian Heaviside smearing in lattice QCD, Phys. Rev. D 83 (2011) 114505, https://doi.org/10.1103/PhysRevD.83.114505, arXiv:1104.3870.

[35] M. Peardon, J. Bulava, J. Foley, C. Morningstar, J. Dudek, R.G. Edwards, B. Joo, H.-W. Lin, D.G. Richards, K.J. Juge, A novel quark-field creation operator construction for hadronic physics in lattice QCD, Phys. Rev. D 80 (2009) 054506, https://doi.org/10.1103/PhysRevD.80.054506, arXiv:0905.2160.

[36] C. Morningstar, M.J. Peardon, Analytic smearing of SU(3) link variables in lattice QCD, Phys. Rev. D 69 (2004) 054501, https://doi.org/10.1103/PhysRevD.69.054501, arXiv:hep-lat/0311018.

[37] J. Foley, K. Jimmy Juge, A. O'Cais, M. Peardon, S.M. Ryan, J.-I. Skullerud, Practical all-to-all propagators for lattice QCD, Comput. Phys. Commun. 172 (2005) 145–162, https://doi.org/10.1016/j.cpc.2005.06.008, arXiv:hep-lat/0505023.

[38] S. Bernardson, P. McCarty, C. Thron, Monte Carlo methods for estimating linear combinations of inverse matrix entries in lattice QCD, Comput. Phys. Commun. 78 (1993) 256–264, https://doi.org/10.1016/0010-4655(94)90004-3.

[39] W. Wilcox, Noise methods for flavor singlet quantities, in: Interdisciplinary Workshop on Numerical Challenges in Lattice QCD, 1999, pp. 127–141, arXiv:hep-lat/9911013.

[40] J. Balog, M. Niedermaier, F. Niedermayer, A. Patrascioiu, E. Seiler, P. Weisz, Comparison of the O(3) bootstrap sigma model with the lattice regularization at low-energies, Phys. Rev. D 60 (1999) 094508, https://doi.org/10.1103/PhysRevD.60.094508, arXiv:hep-lat/9903036.

[41] F. Niedermayer, P. Rufenacht, U. Wenger, Fixed point gauge actions with fat links: scaling and glueballs, Nucl. Phys. B 597 (2001) 413–450, https://doi.org/10.1016/S0550-3213(00)00731-8, arXiv:hep-lat/0007007.

[42] R. Brett, J. Bulava, D. Darvish, J. Fallica, A. Hanlon, B. Hörz, C. Morningstar, Spectroscopy from the lattice: the scalar glueball, AIP Conf. Proc. 2249 (1) (2020) 030032, https://doi.org/10.1063/5.0008566, arXiv:1909.07306.

[43] R.L. Workman, et al., Review of particle physics, PTEP 2022 (2022) 083C01, https://doi.org/10.1093/ptep/ptac097.

[44] B. Grinstein, I.Z. Rothstein, Errors in lattice extractions of alpha-s due to use of unphysical pion masses, Phys. Lett. B 385 (1996) 265–272, https://doi.org/10.1016/0370-2693(96)00832-5, arXiv:hep-ph/9605260.

[45] S. Necco, Universality and scaling behavior of RG gauge actions, Nucl. Phys. B 683 (2004) 137–167, https://doi.org/10.1016/j.nuclphysb.2004.01.032, arXiv:hep-lat/0309017.

[46] F. Knechtli, T. Korzec, B. Leder, G. Moir, Power corrections from decoupling of the charm quark, Phys. Lett. B 774 (2017) 649–655, https://doi.org/10.1016/j.physletb.2017.10.025, arXiv:1706.04982.

[47] N. Brambilla, R.L. Delgado, A.S. Kronfeld, V. Leino, P. Petreczky, S. Steinbeißer, A. Vairo, J.H. Weber, Static energy in $(2+1+1)$-flavor lattice QCD: scale setting and charm effects, Phys. Rev. D 107 (7) (2023) 074503, https://doi.org/10.1103/PhysRevD.107.074503, arXiv:2206.03156.

[48] R. Bruschini, P. González, Diabatic description of charmoniumlike mesons, Phys. Rev. D 102 (7) (2020) 074002, https://doi.org/10.1103/PhysRevD.102.074002, arXiv:2007.07693.

[49] Jülich Supercomputing Centre, JUQUEEN: IBM Blue Gene/Q supercomputer system at the Jülich supercomputing centre, J. Large-Scale Res. Facil. 1 (A1) (2015), https://doi.org/10.17815/jlsrf-1-18.

[50] R.G. Edwards, B. Joo, The Chroma software system for lattice QCD, Nucl. Phys. B, Proc. Suppl. 140 (2005) 832, https://doi.org/10.1016/j.nuclphysbps.2004.11.254, arXiv:hep-lat/0409003.